



**HAL**  
open science

# Surface Kinetic Energy Distributions in the Global Oceans From a High-Resolution Numerical Model and Surface Drifter Observations

Xiaolong Yu, Aurélien L. Ponte, Shane Elipot, Dimitris Menemenlis, Edward D. Zaron, Ryan Abernathey

► **To cite this version:**

Xiaolong Yu, Aurélien L. Ponte, Shane Elipot, Dimitris Menemenlis, Edward D. Zaron, et al.. Surface Kinetic Energy Distributions in the Global Oceans From a High-Resolution Numerical Model and Surface Drifter Observations. *Geophysical Research Letters*, 2019, 46, pp.9757-9766. 10.1029/2019GL083074 . insu-03683190

**HAL Id: insu-03683190**

**<https://insu.hal.science/insu-03683190>**

Submitted on 1 Jun 2022

**HAL** is a multi-disciplinary open access archive for the deposit and dissemination of scientific research documents, whether they are published or not. The documents may come from teaching and research institutions in France or abroad, or from public or private research centers.

L'archive ouverte pluridisciplinaire **HAL**, est destinée au dépôt et à la diffusion de documents scientifiques de niveau recherche, publiés ou non, émanant des établissements d'enseignement et de recherche français ou étrangers, des laboratoires publics ou privés.

Copyright

# Geophysical Research Letters

## RESEARCH LETTER

10.1029/2019GL083074

### Key Points:

- Velocity frequency rotary spectra from a 1/48° global ocean model are compared to spectra derived from hourly surface drifter observations
- The model exhibits variance 4 times higher in the semidiurnal band and 3 times lower in the inertial band compared with drifter data
- Surface drifter observations are valuable for assessment of the surface circulation predicted by tide- and eddy-resolving global models

### Supporting Information:

- Supporting Information S1

### Correspondence to:

X. Yu,  
xiaolong.yu@ifremer.fr

### Citation:

Yu, X., Ponte, A. L., Elipot, S., Menemenlis, D., Zaron, E. D., & Abernathey, R. (2019). Surface kinetic energy distributions in the global oceans from a high-resolution numerical model and surface drifter observations. *Geophysical Research Letters*, 46, 9757–9766. <https://doi.org/10.1029/2019GL083074>

Received 1 APR 2019

Accepted 5 AUG 2019

Accepted article online 9 AUG 2019

Published online 19 AUG 2019

## Surface Kinetic Energy Distributions in the Global Oceans From a High-Resolution Numerical Model and Surface Drifter Observations

Xiaolong Yu<sup>1</sup> , Aurélien L. Ponte<sup>1</sup> , Shane Elipot<sup>2</sup> , Dimitris Menemenlis<sup>3</sup> , Edward D. Zaron<sup>4</sup> , and Ryan Abernathey<sup>5</sup> 

<sup>1</sup>Ifremer, Université de Brest, CNRS, IRD, Laboratoire d'Océanographie Physique et Spatiale, IUEM, Brest, France,

<sup>2</sup>Rosenstiel School of Marine and Atmospheric Sciences, University of Miami, Miami, FL, USA, <sup>3</sup>Jet Propulsion Laboratory, California Institute of Technology, Pasadena, CA, USA, <sup>4</sup>Department of Civil and Environmental Engineering, Portland State University, Portland, OR, USA, <sup>5</sup>Department of Earth and Environmental Sciences, Columbia University, New York, NY, USA

**Abstract** The surface kinetic energy of a 1/48° global ocean simulation and its distribution as a function of frequency and location are compared with the one estimated from 15,329 globally distributed surface drifter observations at hourly resolution. These distributions follow similar patterns with a dominant low-frequency component and well-defined tidal and near-inertial peaks globally. Quantitative differences are identified with deficits of low-frequency energy near the equator (factor 2) and at near-inertial frequencies (factor 3) and an excess of energy at semidiurnal frequencies (factor 4) for the model. Owing to its hourly resolution and its near-global spatial coverage, the array of surface drifters is an invaluable tool to evaluate the realism of tide-resolving high-resolution ocean simulations used in observing system simulation experiments. Sources of bias between model and drifter data are discussed, and associated leads for future work highlighted.

**Plain Language Summary** Ocean currents predominately control the transport and distribution of physical properties (such as heat and momentum) and biochemical tracers (such as carbon, oxygen, and nutrients) in the global oceans. These currents are generally most energetic at the ocean surface and distributed across a broad range of temporal and spatial scales. Global ocean models simulate ocean variability from large-scale circulations to tidal motions and are used to provide guidance for new global oceanographic observations, especially for future high-resolution satellite missions. Therefore, it is crucial to assess the realism of global ocean models. In this study, we use drifter observations of global surface currents to compare with the output from a 1/48° global ocean simulation. Our results show that the model exhibits a broad qualitative consistency with the surface drifter data but also displays some key differences at high-frequency dynamics. The model shows a 3 times deficit of near-inertial variance and a 4 times excess of semidiurnal variance when compared with surface drifter data. Our findings demonstrate that the global drifter data set with hourly temporal resolution provides a resource for assessment of the surface circulation predicted by state-of-the-art global ocean models.

## 1. Introduction

Satellite remote sensing has been extensively used to advance our understanding of ocean dynamics over the last several decades (Fu et al., 2018; Morrow & Le Traon, 2012). With the advent of wide-swath radar interferometry, the upcoming Surface Water and Ocean Topography (SWOT) mission is expected to measure, for the first time, the sea surface height globally and at spatial scales down to 15–50 km depending on the local sea state (Callies & Wu, 2019; Morrow et al., 2019; Wang et al., 2019). It is anticipated that these unprecedented sea surface height measurements will capture ocean variability in the submesoscale range (Durand et al., 2010; Fu & Ubelmann, 2014). However, one common issue with altimetric data, as well as with other types of satellite observations in general, arises from the long repeat sampling cycles and therefore limited temporal resolution which complicates the disentanglement of signals with different temporal scales (e.g., slow balanced geostrophic motions and fast unbalanced internal gravity waves; Chavanne & Klein, 2010). The issue of temporal sampling is critical for the SWOT mission (21-day repeat sampling) and other satellite

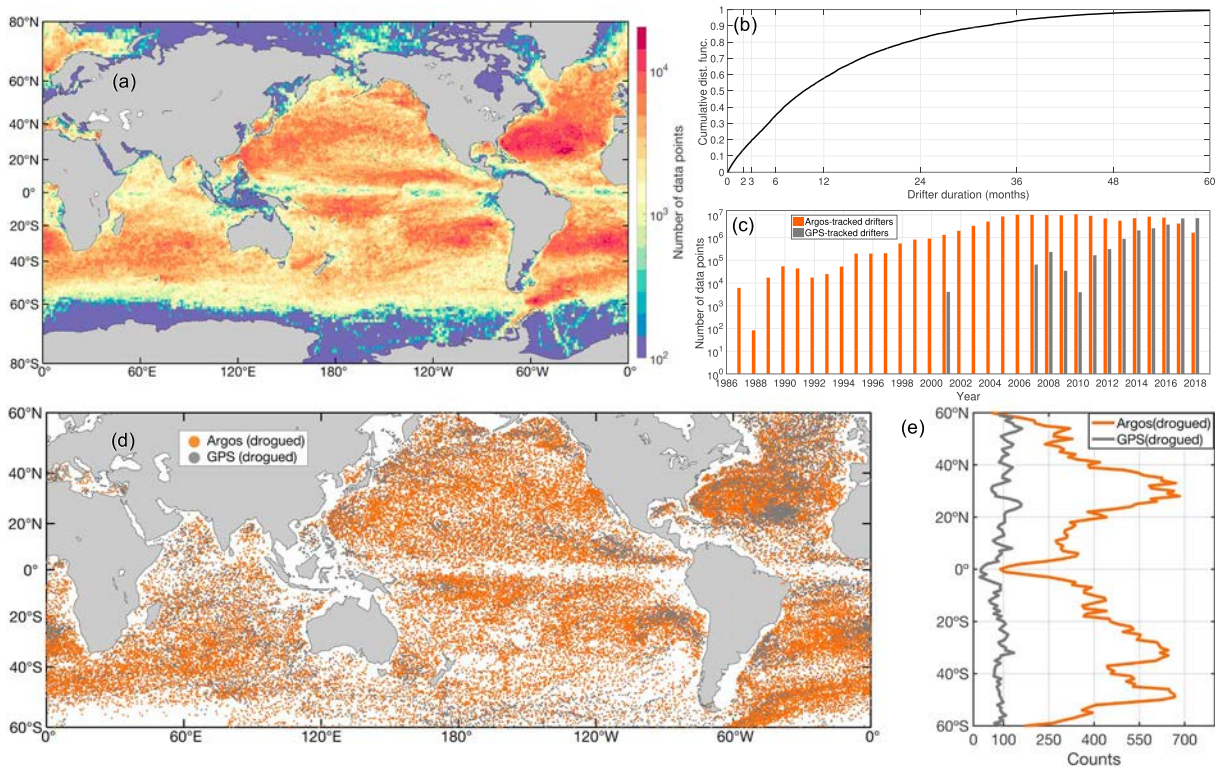


**Figure 1.** (a) Number of hourly drifter data points in  $1^\circ \times 1^\circ$  bins for the period from October 1987 to November 2018. (b) Cumulative distribution function of drifter trajectory duration. (c) Histogram of years of hourly data points collected from Argos- and GPS-tracked surface drifters. (d) Mean location of drogued drifter in 60-day trajectory segments overlapping by 50%. Argos- and GPS-tracked drifters are indicated by orange and gray, respectively. (e) Number of drifter segments tracked by Argos (orange) and GPS (gray) as a function of latitude.

missions that are under development such as the Surface KInematic Monitoring (SKIM) mission (Ardhuin et al., 2018).

Tide-resolving global numerical models with kilometer-scale resolution are revolutionizing our view of a variety of ocean processes (e.g., Arbic et al., 2018; Su et al., 2018) and provide a useful testing ground to investigate potential opportunities and challenges for oceanographic observations (e.g., Wang et al., 2018). In particular, efforts to unravel the issue of balance/unbalanced disentanglement in the SWOT mission have heavily relied on high-resolution global numerical simulations (Qiu et al., 2018; Savage et al., 2017; Torres et al., 2018). This then leads to another important question: How realistic are these state-of-the-art global ocean simulations?

To assess the realism of ocean variability predicted by global ocean simulations, in situ observations with the requisite resolution and (near-)global coverage are important. Elipot et al. (2016) produced a unique global data set of surface drifter positions and velocities with hourly temporal resolution, which enables studies of near-surface high-frequency motion (e.g., inertial and tidal). The surface drifter measurements have been previously used to investigate a wide range of oceanic processes and dynamics, from global velocity climatology (Lumpkin & Johnson, 2013) and mesoscale coherent vortices (Lumpkin, 2016) to submesoscale motions (Lumpkin & Elipot, 2010; Zhang & Qiu, 2018), near-inertial waves (Elipot et al., 2010; Liu et al., 2019), internal tides (Zaron, 2019), and relative dispersion (Corrado et al., 2017). In situ observations by oceanographic moorings or profiling instruments may be suited to obtaining depth-dependent tidal and higher-frequency variability for model assessment (e.g., Ansong et al., 2017; Savage et al., 2017) and thus complement surface drifter observations.

In this study, we address the aforementioned question by comparing a global ocean model with global surface drifter measurements via frequency rotary velocity spectrum diagnostics, thus focusing on surface kinetic energy (KE). We take advantage of the drifter data set growth and development, in particular for drifters tracked by the Global Positioning System (GPS), which have improved position accuracy and

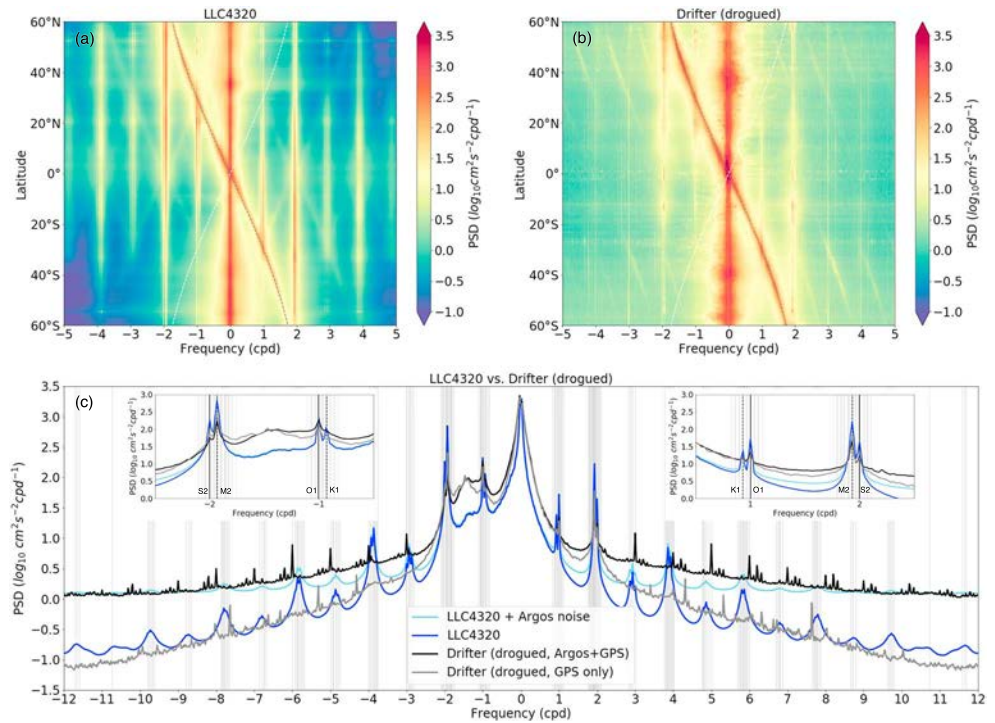


**Figure 2.** Zonally averaged rotary frequency spectra in  $1^\circ$  latitude bins from surface velocity fields of (a) the LLC4320 simulation and (b) drogued drifter data. The inertial frequency ( $-f/2\pi$  cpd) is indicated by the gray dashed line, and the Coriolis frequency ( $f/2\pi$  cpd) is indicated by the white dashed line. (c) Globally averaged anticyclonic (at negative frequencies) and cyclonic (at positive frequencies) spectra of the LLC4320 simulation (blue) and the drogued drifter (black) horizontal velocity. The spectra estimated from only GPS-tracked drogued drifters are shown as gray lines. The light blue lines give the LLC4320 spectra calculated after adding Argos white noise level as described in section 3. Vertical light gray lines correspond to astronomical tidal frequencies. The insets are a zoom for frequencies from  $-2.5$  to  $-0.5$  cpd (top left) and from  $0.5$  to  $2.5$  cpd (top right), respectively.

increased time resolution in comparison with those tracked by the Argos system (Lumpkin et al., 2017). Our results indicate surface drifters may be useful for comparing and assessing numerical ocean models, from subinertial to supertidal frequencies.

## 2. Data and Methods

### 2.1. High-Resolution Global Model

Here, we use output from a state-of-the-art global ocean model, the so-called LLC4320 simulation (Su et al., 2018), which was performed using the Massachusetts Institute of Technology general circulation model (MITgcm; Marshall et al., 1997) with a horizontal grid spacing of  $1/48^\circ$  and 90 vertical levels. The simulation was carried out on a global Latitude-Longitude-polar Cap (LLC) grid (Forget et al., 2015) in a hydrostatic configuration, for a duration of 14 months from 13 September 2011 to 15 November 2012. The initial model state is derived from a  $1/6^\circ$  global ocean state estimate from the Estimating the Circulation and Climate of the ocean, Phase II, output (Menemenlis et al., 2008), and then a set of the LLC simulations were sequentially developed with increasing resolutions of  $1/12^\circ$ ,  $1/24^\circ$ , and finally  $1/48^\circ$ . The model is forced by surface flux fields (with a time interval of 6 hr starting in 2011) from the  $0.14^\circ$  European Centre for Medium-Range Weather Forecasting atmospheric operational model analysis, which include 10-m wind velocity, 2-m air temperature and humidity, downwelling long and shortwave radiation, and atmospheric pressure load (Dee et al., 2011). More important, the model has a tidal forcing that includes the 16 major constituents. The model resolves mesoscale eddies and internal waves and permits submesoscale variability. Horizontal wavenumber spectra suggest that the effective resolution of LLC4320 is about 8 km (Rocha et al., 2016). The model time step is 25 s, and model variables are stored as snapshots at hourly intervals. The present study focuses on a yearlong record of surface horizontal velocity fields, starting on 15 November 2011.

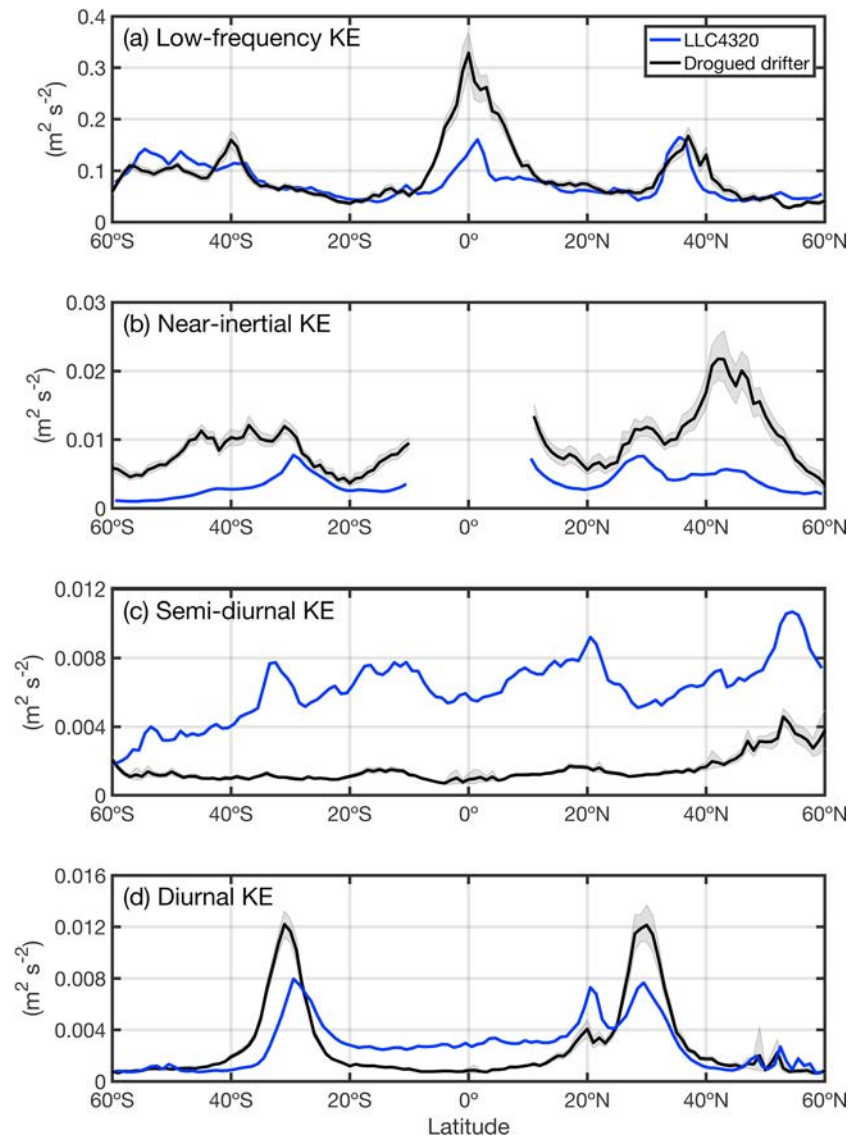


**Figure 3.** Zonally averaged (a) low-frequency, (b) near-inertial, (c) semidiurnal, and (d) diurnal KE in  $1^\circ$  latitude bins estimated from the model (blue) and drogued drifter data (black). The colored shading shows the 95% confidence interval determined using a bootstrapping resampling approach. Note that near-inertial KE at latitude range  $10^\circ\text{S}$  to  $10^\circ\text{N}$  is not included because inertial motions there are indistinguishable from low-frequency variability in the spectra. KE = kinetic energy.

## 2.2. Surface Drifter Observations

For comparison, we use the latest version of the hourly data set from the Global Drifter Program (version 1.02, data available at [http://www.aoml.noaa.gov/phod/gdp/hourly\\_data.php](http://www.aoml.noaa.gov/phod/gdp/hourly_data.php)). The data set comprises horizontal velocity and position estimates at hourly intervals (Elipot et al., 2016) from 15,329 individual surface drifter trajectories for a period from October 1987 to November 2018. Because the drifters are scattered throughout the open ocean worldwide, the spatial distribution of the drifter hourly data points is somewhat inhomogeneous (Figure 1a). Preferentially sampled regions can be found in the convergence zones, such as the interior of subtropical gyres. In contrast, areas with a divergent circulation, such as the equatorial region, and polar and coastal regions are generally less sampled. The overall average lifetime of surface drifters in the ocean is about 404 days, with up to 86% and 40% of the drifter duration longer than 60 days and a year, respectively (Figure 1b). The data set contains both surface drifter trajectories tracked by the Argos system and by the GPS (Figure 1c). In particular, GPS-tracked drifters have been more heavily deployed after 2012 and account for 19.8% of the available data points.

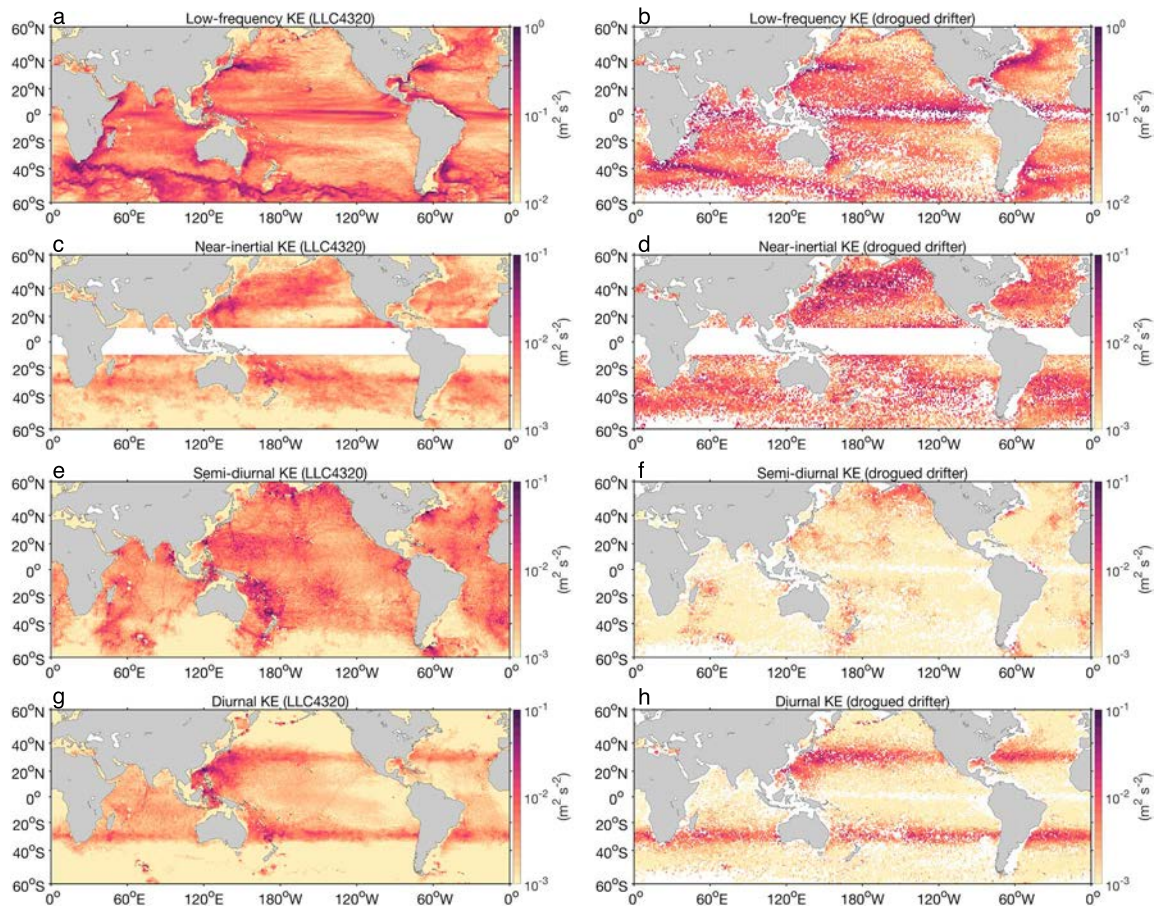


**Figure 4.** Global maps of the (a, b) low-frequency, (c, d) near-inertial, (e, f) semidiurnal, and (g, h) diurnal KE in  $1^\circ \times 1^\circ$  bins estimated from the LLC4320 simulation (left column) and drogued drifter data (right column). KE = kinetic energy.

The drifter observations provide a rich data set that, because of its Lagrangian nature, convolves both spatial and temporal variability as the drifters passively follow ocean currents. Accuracy of drifter position and velocity estimates is largely determined by the tracking system (i.e., Argos versus GPS; Elipot et al., 2016). Furthermore, it should be noted that wind slippage effects may introduce a bias between the drifter speed and the surface flow speed (Lumpkin & Pazos, 2007). In order to minimize potential wind slippage effects, this study exclusively considers drifters that are drogued, which consist of 61 million hourly current vectors (about 40.0% of the available data). Drogued drifter currents are expected to be representative of currents at the drogue depth, that is, 15 m, which may be a source of potential discrepancy when these currents are compared to surface model ones as discussed in section 4.

### 2.3. Frequency Rotary Spectrum

Surface horizontal velocity time series from the LLC4320 simulation are used to estimate rotary spectra of horizontal velocity at each model grid point. For observations, rotary spectra are computed from horizontal velocities along drifter trajectories. For both data sets, we first divide velocity time series into segments of 60 days overlapping by 50% and linearly detrend over each segment, and then we compute the 1-D discrete Fourier transform of complex-valued fields ( $u + iv$ , where  $u$  and  $v$  are zonal and meridional velocity, respectively) multiplied by a Hanning window. The spectra are formed by multiplying the Fourier coefficients by their complex conjugates, and the spectra are averaged over segments. When averaged in space, drifter spectra are associated with the mean latitude and longitude of each trajectory segment (Figure 1d). Given the geographical distribution of surface drifters, velocity data in coastal waters with depth shallower than 500 m and polar regions with latitude higher than  $60^\circ$  are not considered in the calculation for both data sets.

We also integrate rotary frequency spectral densities over four frequency bands to compute KE components of interest, including high-frequency ( $>0.5$  cpd, absolute values here and hereinafter), near-inertial

(0.9–1.1 $f$ ), semidiurnal (1.9–2.1 cpd), and diurnal (0.9–1.1 cpd). The KE components estimated from windowed spectra are then multiplied by a factor of 8/3 to compensate for the Hanning windowing operation (Emery & Thomson, 2001). Total KE is estimated from temporal averages of instantaneous fields, and low-frequency KE is computed as total KE minus high-frequency KE. To achieve a balance between the drifter data point density (Figure 1e) and latitudinal variability of the bin-averaged variables, a bin size of 1° latitude is employed to compare zonally averaged rotary spectra and the associated band integrals between the model and drifter data (Figures 2 and 3, respectively). The uncertainties of bin-averaged KE values are estimated as 95% confidence intervals via a bootstrap method (Efron & Gong, 1983). Finally, the band-integrated KE estimates are averaged in 1° × 1° spatial bins in Figure 4.

### 3. Results

The model and drifter rotary spectra show qualitatively comparable distributions of energy as a function of frequency and latitude, characterized by high-energy peaks at low frequencies (<0.5 cpd) and diurnal, semidiurnal, and latitude-varying inertial frequencies (Figures 2a and 2b). A noticeable difference is that semidiurnal signals have a higher spectral peak than near-inertial signals in almost all latitudinal bands in the model, while drifters show the opposite. Furthermore, model rotary spectra show an elevated energy level at tidal frequencies compared to drifter ones (also see Figure S1 in the supporting information).

Globally averaged rotary spectra show prominent peaks corresponding to the diurnal and semidiurnal tides (Figure 2c). At low frequencies, the model spectral densities are smaller than those estimated from drifter data, indicating an overall deficit of low-frequency KE variance in the model. Another notable difference is the spectral slope at supertidal frequencies, as the drifter spectra (black line) exhibit a flatter slope than the model (blue line). This flatter spectrum is caused by the predominance of Argos-tracked drifters and the associated larger position and velocity noise levels. We use the spectral value at the highest frequencies, 1.1 cm<sup>2</sup>·s<sup>-2</sup>·cpd<sup>-1</sup> at 12 cpd, as a drifter white noise level. The velocity variance associated with the white noise is calculated by integrating 1.1 cm<sup>2</sup>·s<sup>-2</sup>·cpd<sup>-1</sup> over the whole spectral frequency range (–12 cpd, 12 cpd), yielding a value of 26.4 cm<sup>2</sup>/s<sup>2</sup>. This velocity variance corresponds to a mean velocity error value of 5.1 cm/s for drifters, which is approximately consistent with the average drifter velocity noise (Figure S2). We artificially add this constant white noise spectrum to the model results, and the recalculated rotary spectra (light blue line) display a very weak slope, comparative to the drifter spectra. By contrast, globally averaged spectra estimated from only GPS-tracked drifters display a much steeper slope and better match with the model results, suggesting that the effect of the noise associated with Argos-tracked drifters is substantial. Furthermore, tidal harmonics with frequencies higher than semidiurnal line up with peaks in the model-derived spectra but not those from drifters. The mismatch between drifter-derived spectral peaks and high-frequency tidal harmonics was also seen in Elipot et al. (2016) and remains unexplained. The model energy level of troughs in between overtones are lower than drifters. Potential sources explaining these discrepancies may be the following: a lack of spatial resolution which may inhibit the emergence of an internal wave continuum (Muller et al., 2015; Savage et al., 2017), a difference of perspective (e.g., Lagrangian vs Eulerian, see the discussion), a deficit of high-frequency energy in the atmospheric forcing, or combined effects of each source of discrepancy.

#### 3.1. Low-Frequency Variance

Model and drifter low-frequency KE agree within a factor of less than 1.5 away from the equatorial band (10°S to 10°N; Figure 3a). Within the equatorial region, the model-averaged low-frequency KE is lower than the value inferred from drifters by a factor of 2. This factor mirrors the relative amplitude of peak energies: 0.15 m<sup>2</sup>/s<sup>2</sup> for the model versus 0.34 m<sup>2</sup>/s<sup>2</sup> for drifters. The locations of low-frequency maxima coincide with the latitudes of the equatorial ocean, the Kuroshio and the Gulf Stream (30–40°N), and the Antarctic Circumpolar Current (40–55°S). For other regions, mostly the interior of the subtropical and subpolar gyres, there is little latitudinal variability with most values slightly smaller than 0.1 m<sup>2</sup>/s<sup>2</sup>. Low-frequency KE accounts for over 80% of the total KE, both for the model and drifter data, consistent with the expected dominant reservoir of KE at the mesoscale (Ferrari & Wunsch, 2009). The band-integrated variances averaged in 1° × 1° bins indicate that model and drifter low-frequency surface motions exhibit both comparable spatial distributions and levels of energy (Figures 4a and 4b). Note that the smaller number of drifters in the Pacific and Atlantic equatorial regions for the hourly data set prevents the identification of spatial patterns whose existence is suggested by model energy maps (also seen in Figure 1e).

### 3.2. High-Frequency Variance

Surface KE associated with diurnal and semidiurnal tides and near-inertial waves are all 1 order of magnitude smaller than low-frequency KE. Near-inertial KE is the second largest component in the drifter data and shows an intensification at midlatitudes (i.e., 30–60°N and 30–60°S), especially in the Northern Hemisphere (Figure 3b). In contrast, the model does not show much variance associated with near-inertial motions. The model underestimates by a factor of 3 (an average over 60°S to 60°N) near-inertial variance compared with the drifter observations, most likely due to the coarse temporal resolution (6-hourly) of the atmospheric forcing in the model (Klein et al., 2004; Rimac et al., 2013). Other possibilities such as low storm activity for the single year analyzed by the model and a too-deep model mixed layer may also be at play. Note that this deficit is most evident at midlatitudes and gradually reduces at latitudes smaller than 30°. This is consistent with the findings of Rimac et al. (2013), who used a global eddy-permitting model forced by wind stress of different temporal resolutions to demonstrate that near-inertial KE at midlatitudes is more sensitive to wind forcing than in the tropical and subtropical regions. Global maps indicate that those intensified near-inertial variance levels are in common midlatitude storm-track regions (e.g., North Pacific/Atlantic; Figures 4c and 4d). Interestingly, near-inertial signals in the model are muted in most areas of the Southern Ocean but not in the corresponding latitude range in the Northern Hemisphere, probably due to the poor representation of atmospheric fields from the European Centre for Medium-Range Weather Forecasting reanalysis data in the Southern Ocean (Yuan, 2004).

For semidiurnal KE, the model is larger by a factor of 4 compared to drifters when averaged within 60°S to 60°N (Figure 3c), and this result is insensitive to the choice of the semidiurnal band limits. The enhancement of the semidiurnal KE by the model is ubiquitous over the global ocean (Figures 4e and 4f). The overestimation of KE in the semidiurnal band in the model may stem from several potentially combined sources, such as absence of topographic internal wave drag (Ansong et al., 2015; Arbic et al., 2010) and insufficient spatial resolution and therefore energy scattering to the wave continuum (Muller et al., 2015; Shriver et al., 2012). Investigation of the origin of the overly large semidiurnal tides in the model is beyond the scope of the present work, but there is also some speculation that it may be caused, in part, by a mistake in the implementation of the load tide and ocean self-attraction. The MITgcm tidal forcing will be documented extensively in a paper in preparation, led by J. Ansong and B. Arbic. The differences reported here, between modeled and observed currents, thus provide a snapshot of the present implementation of the MITgcm, and they will evolve as future improvements are implemented.

Drifters and the model exhibit similar meridional distributions of diurnal KE with an equatorial plateau surrounded by two energy maxima near  $\pm 30^\circ$  latitudes where the local inertial frequency coincides with diurnal frequencies (Figures 3d, 4g, and 4h). The enhanced diurnal energies at the critical latitude are found to be primarily associated with anticyclonic motions (not shown). This is consistent with the finding of Simpson et al. (2002), who used mooring measurements obtained at a location close to the critical latitude in the Southern Hemisphere to demonstrate that motions in the diurnal-inertial band are dominated by anticyclonic oscillatory flows, generated by daily variations in wind stress. A secondary peak of energy around 20°N matches with the latitude of the Luzon Strait, which is a well-known site of strong diurnal internal wave activity (Alford et al., 2015). In the latitude band where diurnal internal tides are free to propagate, that is, between 30°S and 30°N, the diurnal KE computed from the drifter data is slightly less than the diurnal KE from the model. This suggests that the same mechanisms responsible for the excess of semidiurnal energy in the model apply in this area for the diurnal variability.

## 4. Discussion and Perspectives

In this study, surface drifter observations are used for the first time for assessment of the surface circulation predicted by a tide- and eddy-resolving global ocean model. Our results show that the high-resolution simulation exhibits a broad qualitative consistency with surface drifters through a rotary spectral analysis of near-surface velocities on a near-global scale. Several quantitative differences were highlighted: a deficit of model near-inertial variance presumably due to the limited temporal resolution of the atmospheric forcing, an excess of model energy at tidal frequencies, and a deficit of model low-frequency KE near the equator (also see Figure S3). The global drifter data set may thus enable the assessment of the surface circulation predicted by tide-resolving and submesoscale-permitting ocean global numerical simulations. This assessment remains a challenge today (Arbic et al., 2018) and would be timely given the intensive use of these simulations in satellite (SWOT and SKIM) observing system simulation experiments.

In its present form, a test of model's skill based on comparisons between Eulerian and Lagrangian spectra and band-integrated levels is, however, limited by uncertainties around several underlying assumptions: equivalence between model Eulerian spectra and band-integrated levels and drifter Lagrangian ones, weak vertical shear between model top most bin (of the order of a meter) and drifter drogue depths (15m), and long-term stationarity of rotary spectra (i.e., the model analysis is based on 1 year of data, whereas the drifter data analysis is based on multiple years). Testing of these assumptions is left for future studies.

Under suitable assumptions (e.g., turbulent, isotropic, stationary, and nondivergent flows), the correspondence between Lagrangian and Eulerian spectra depends on a parameter  $\alpha = U_{\text{rms}} T_E / L_E$ , where  $U_{\text{rms}}$  is the root-mean-square of the velocity and  $T_E$  and  $L_E$  are the temporal and spatial decorrelation scales, respectively (Davis, 1983; Middleton, 1985). A small  $\alpha$  corresponds to a "fixed float" regime: Drifters behave like moorings, and Eulerian and Lagrangian spectra are equal. For moderate to large values of  $\alpha$ , the Eulerian field spatial variability is aliased into the temporal Lagrangian one and Lagrangian spectra differ from Eulerian ones, potentially resembling broadened versions of the latter (Davis, 1983; Middleton, 1985). Both small and moderate values of  $\alpha$  are found in the ocean (Lumpkin et al., 2002). Comparisons of Eulerian and Lagrangian spectral shapes should therefore be limited to areas with reduced  $\alpha$ , which has not been attempted here. In regions with higher  $\alpha$ , the model/drifter comparison may have to be limited to bulk diagnostics and/or diagnostics for which an Eulerian/Lagrangian correspondence exists (e.g., mean velocities and eddy KE; see Laurindo et al., 2017).

Small-scale waves, on the other hand, may be sensitive to Doppler frequency shifting by lower-frequency currents and have thus been expected to exhibit more compact frequency distributions in Lagrangian space and to be more easily identifiable there (Nagai et al., 2015; Shakespeare & Hogg, 2017). Interestingly, the Doppler frequency shift equals the wave frequency times  $UT_w / L_w$ , where  $U$  is the lower-frequency current amplitude,  $T_w$  the wave period, and  $L_w$  the wave length (note the similarity with  $\alpha$ ). But wave-low-frequency flow interactions do not reduce to Doppler frequency shifts in general (Dunphy et al., 2017) and other Eulerian-Lagrangian spectral relationships are expected. For example, more compact Eulerian frequency distributions may be expected when wave propagation is not affected by a lower-frequency current, a scenario whose actual occurrence would have to be confirmed. Idealized and realistic numerical studies would be necessary in order to decide where (geographically), when (in terms of process amplitudes and scales), and how (quantitatively) Lagrangian and Eulerian spectra and band energy levels correspond.

Vertical shear and wind slippage, which have been both ignored here, may also limit the comparison between model surface currents and drifter currents. In order to partially address this issue, a comparison between drogued and undrogued spectra and band-integrated energies is presented in supporting information (Figures S4–S5) and shows that differences are modest in comparison to the differences between model and drogued drifter spectra. Further, we also assessed the differences of spectra between surface and 15-m velocities using the model output in a regional domain (290×260 km) of the northeast Atlantic (not shown). We find that the surface spectrum is only slightly augmented at low frequencies (on average by about 12%) compared to the one at 15 m and therefore conclude that the main findings of this paper, especially for variances at high frequencies, are not affected.

The most natural road for improvement in order to effectively test the skill of numerical simulations with the global drifter data set would be to compute drifter trajectories from these simulations. Wind slippage, drag distributions, and presence of drogue or not, could be accounted for. Such release would allow the computation of model Lagrangian frequency spectra which could be directly compared with observed ones. This option raises several technical questions regarding appropriate model output frequency (for an offline analysis) and spatiotemporal interpolation schemes (Zouari & Babiano, 1990).

The noise associated with positional data provided by Argos system appears as a limit for the investigation of oceanic motions at frequencies above the semidiurnal one. Fortunately, the fraction of GPS-tracked drifters in the Global Drifter Program will continue to grow in the years to come, which will be beneficial for studies of supertidal motions (Lumpkin, 2016). Time-averaged divergence areas such as the equatorial ocean will likely remain undersampled, however. If correctly instrumented, moorings such as those developed in equatorial networks may mitigate such sampling issue (Bonjean & Lagerloef, 2002).

Finally, the observation of high-frequency variability in drifter trajectories should be a reminder that these instruments may, despite their inhomogeneous spatial coverage compared to satellite data, represent

valuable in situ observations in order to disentangle slow and fast variability in satellite data. This disentanglement will be a challenge for SWOT (Ponte et al., 2017). It will probably be a larger one for SKIM where near-inertial waves contamination will be more significant than for SWOT (Ardhuin et al., 2018). Fortunately for SKIM, it will measure currents, that is, the same variable readily deduced from drifter trajectories. This may turn out to be an advantage in order to distinguish fast and slow motions in SKIM data.

#### Acknowledgments

This work was carried out as part of the ANR project number 17-CE01-0006-01 entitled EQUINOx (Disentangling Quasi-geostrophic Motions and Internal Waves in High Resolution Satellite Observations of the Ocean). It is also part of the CNES-TOSCA project entitled “New Dynamical Tools for submesoscale characterization in SWOT data” that was proposed within the context of the SWOT mission. Shane Elipot is supported by the National Science Foundation under Grant 1851166. The surface drifter data are collected and archived by the NOAA Global Drifter Program ([http://www.aoml.noaa.gov/phod/gdp/hourly\\_data.php](http://www.aoml.noaa.gov/phod/gdp/hourly_data.php)). The LLC output is available from the ECCO project ([http://ecco2.org/llc\\_hires](http://ecco2.org/llc_hires)).

#### References

- Alford, M. H., Peacock, T., MacKinnon, J. A., Nash, J. D., Buijsman, M. C., Centurioni, L. R., et al. (2015). The formation and fate of internal waves in the South China Sea. *Nature*, *521*(7550), 65–69.
- Ansong, J. K., Arbic, B. K., Alford, M. H., Buijsman, M. C., Shriver, J. F., Zhao, Z. X., et al. (2017). Semidiurnal internal tide energy fluxes and their variability in a global ocean model and moored observations. *Journal of Geophysical Research: Oceans*, *122*, 1882–1900. <https://doi.org/10.1002/2016jc012184>
- Ansong, J. K., Arbic, B. K., Buijsman, M. C., Richman, J. G., Shriver, J. F., & Wallcraft, A. J. (2015). Indirect evidence for substantial damping of low-mode internal tides in the open ocean. *Journal of Geophysical Research: Oceans*, *120*, 6057–6071. <https://doi.org/10.1002/2015jc010998>
- Arbic, B., Alford, M. H., Ansong, J. K., Buijsman, M. C., Ciotti, R. B., Farrar, J. T., et al. (2018). A primer on global internal tide and internal gravity wave continuum modeling in HYCOM and MITgcm. In E. P. Chassignet, A. Pascual, J. Tintoré, & J. Verron (Eds.), *New frontiers in operational oceanography* (pp. 307–392): GODAE OceanView.
- Arbic, B., Wallcraft, A. J., & Metzger, E. J. (2010). Concurrent simulation of the eddying general circulation and tides in a global ocean model. *Ocean Modelling*, *32*(3–4), 175–187.
- Ardhuin, F., Aksenov, Y., Benetazzo, A., Bertino, L., Brandt, P., Caubet, E., et al. (2018). Measuring currents, ice drift, and waves from space: The sea surface kinematics multiscale monitoring (SKIM) concept. *Ocean Science*, *14*(3), 337–354.
- Bonjean, F., & Lagerloef, G. S. E. (2002). Diagnostic model and analysis of the surface currents in the tropical Pacific Ocean. *Journal of Physical Oceanography*, *32*(10), 2938–2954.
- Callies, J., & Wu, W. (2019). Some expectations for submesoscale sea surface height variance spectra. *Journal of Physical Oceanography*. <https://doi.org/10.1175/JPO-D-18-0272.1>
- Chavanne, C. P., & Klein, P. (2010). Can oceanic submesoscale processes be observed with satellite altimetry? *Geophysical Research Letters*, *37*, L22602. <https://doi.org/10.1029/2010gl045057>
- Corrado, R., Lacorata, G., Palatella, L., Santoleri, R., & Zambianchi, E. (2017). General characteristics of relative dispersion in the ocean. *Scientific Reports*, *7*, 46291.
- Davis, R. (1983). Oceanic property transport, Lagrangian particle statistics, and their prediction. *Journal of Marine Research*, *41*(1), 163–194.
- Dee, D. P., Uppala, S. M., Simmons, A. J., Berrisford, P., Poli, P., Kobayashi, S., et al. (2011). The ERA-Interim reanalysis: Configuration and performance of the data assimilation system. *Quarterly Journal of the Royal Meteorological Society*, *137*(656), 553–597.
- Dunphy, M., Ponte, A. L., Klein, P., & Le Gentil, S. (2017). Low-mode internal tide propagation in a turbulent eddy field. *Journal of Physical Oceanography*, *47*(3), 649–665.
- Durand, M., Fu, L. L., Lettenmaier, D. P., Alsdorf, D. E., Rodriguez, E., & Esteban-Fernandez, D. (2010). The Surface Water and Ocean Topography mission: Observing terrestrial surface water and oceanic submesoscale eddies. *Proceedings of the IEEE*, *98*(5), 766–779.
- Efron, B., & Gong, G. (1983). A leisurely look at the bootstrap, the jackknife, and cross-validation. *American Statistician*, *37*(1), 36–48.
- Elipot, S., Lumpkin, R., Perez, R. C., Lilly, J. M., Early, J. J., & Sykulski, A. M. (2016). A global surface drifter data set at hourly resolution. *Journal of Geophysical Research: Oceans*, *121*, 2937–2966. <https://doi.org/10.1002/2016jc011716>
- Elipot, S., Lumpkin, R., & Prieto, G. (2010). Modification of inertial oscillations by the mesoscale eddy field. *Journal of Geophysical Research*, *115*, C09010. <https://doi.org/10.1029/2009jc005679>
- Emery, W. J., & Thomson, R. E. (2001). Chapter 5—Time-series analysis methods, *Data analysis methods in physical oceanography* (pp. 371–567). Elsevier Science.
- Ferrari, R., & Wunsch, C. (2009). Ocean circulation kinetic energy: Reservoirs, sources, and sinks. *Annual Review of Fluid Mechanics*, *41*, 253–282.
- Forget, G., Campin, J. M., Heimbach, P., Hill, C. N., Ponte, R. M., & Wunsch, C. (2015). ECCO version 4: An integrated framework for non-linear inverse modeling and global ocean state estimation. *Geoscientific Model Development*, *8*(10), 3071–3104.
- Fu, L. L., Lee, T., Liu, W. T., & Kwok, R. (2018). 50 years of satellite remote sensing of the ocean. *Meteorological Monographs*, *59*, 5.1–5.46.
- Fu, L. L., & Ubelmann, C. (2014). On the transition from profile altimeter to swath altimeter for observing global ocean surface topography. *Journal of Atmospheric and Oceanic Technology*, *31*(2), 560–568.
- Klein, P., Lapeyre, G., & Large, W. G. (2004). Wind ringing of the ocean in presence of mesoscale eddies. *Geophysical Research Letters*, *31*, L15306. <https://doi.org/10.1029/2004gl020274>
- Laurindo, L. C., Mariano, A. J., & Lumpkin, R. (2017). An improved near-surface velocity climatology for the global ocean from drifter observations. *Deep-Sea Research Part I-Oceanographic Research Papers*, *124*, 73–92.
- Liu, Y., Jing, Z., & Wu, L. (2019). Wind power on oceanic near-inertial oscillations in the global ocean estimated from surface drifters. *Geophysical Research Letters*, *46*, 2647–2653. <https://doi.org/10.1029/2018GL081712>
- Lumpkin, R. (2016). Global characteristics of coherent vortices from surface drifter trajectories. *Journal of Geophysical Research: Oceans*, *121*, 1306–1321. <https://doi.org/10.1029/2018gl081712>
- Lumpkin, R., & Elipot, S. (2010). Surface drifter pair spreading in the North Atlantic. *Journal of Geophysical Research*, *115*, C12017. <https://doi.org/10.1029/2010jc006338>
- Lumpkin, R., & Johnson, G. C. (2013). Global ocean surface velocities from drifters: Mean, variance, El Niño–Southern Oscillation response, and seasonal cycle. *Journal of Geophysical Research: Oceans*, *118*, 2992–3006. <https://doi.org/10.1002/jgrc.20210>
- Lumpkin, R., Ozgokmen, T., & Centurioni, L. (2017). Advances in the application of surface drifters. *Annual Review of Marine Science*, *9*, 59–81.
- Lumpkin, R., & Pazos, M. (2007). *Measuring surface currents with SVP drifters* (pp. 39–67). Cambridge: Cambridge University Press.
- Lumpkin, R., Treguier, A.-M., & Speer, K. (2002). Lagrangian eddy scales in the northern Atlantic Ocean. *Journal of physical oceanography*, *32*(9), 2425–2440.

- Marshall, J., Adcroft, A., Hill, C., Perelman, L., & Heisey, C. (1997). A finite-volume, incompressible Navier Stokes model for studies of the ocean on parallel computers. *Journal of Geophysical Research*, *102*, 5753–5766. <https://doi.org/10.1029/96jc02775>
- Menemenlis, D., Campin, J., Heimbach, P., Hill, C., Lee, T., Nguyen, A., et al. (2008). ECCO2: High resolution global ocean and sea ice data synthesis. *Mercator Ocean Quarterly Newsletter*, *31*, 13–21.
- Middleton, J. F. (1985). Drifter spectra and diffusivities. *Journal of Marine Research*, *43*(1), 37–55.
- Morrow, R., Fu, L. L., Arduin, F., Benkiran, M., Chapron, B., Cosme, E., et al. (2019). Global observations of fine-scale ocean surface topography with the Surface Water and Ocean Topography (SWOT) mission. *Frontiers in Marine Science*, *6*, 232.
- Morrow, R., & Le Traon, P. Y. (2012). Recent advances in observing mesoscale ocean dynamics with satellite altimetry. *Advances in Space Research*, *50*(8), 1062–1076.
- Muller, M., Arbic, B. K., Richman, J. G., Shriver, J. F., Kunze, E. L., Scott, R. B., et al. (2015). Toward an internal gravity wave spectrum in global ocean models. *Geophysical Research Letters*, *42*, 3474–3481. <https://doi.org/10.1002/2015gl063365>
- Nagai, T., Tandon, A., Kunze, E., & Mahadevan, A. (2015). Spontaneous generation of near-inertial waves by the Kuroshio front. *Journal of Physical Oceanography*, *45*(9), 2381–2406.
- Ponte, A. L., Klein, P., Dunphy, M., & Le Gentil, S. (2017). Low-mode internal tides and balanced dynamics disentanglement in altimetric observations: Synergy with surface density observations. *Journal of Geophysical Research: Oceans*, *122*, 2143–2155. <https://doi.org/10.1002/2016jc012214>
- Qiu, B., Chen, S., Klein, P., Wang, J., Torres, H., Fu, L.-L., & Menemenlis, D. (2018). Seasonality in transition scale from balanced to unbalanced motions in the world ocean. *Journal of Physical Oceanography*, *48*(3), 591–605.
- Rimac, A., von Storch, J. S., Eden, C., & Haak, H. (2013). The influence of high-resolution wind stress field on the power input to near-inertial motions in the ocean. *Geophysical Research Letters*, *40*, 4882–4886. <https://doi.org/10.1002/grl.50929>
- Rocha, C. B., Chereskin, T. K., Gille, S. T., & Menemenlis, D. (2016). Mesoscale to submesoscale wavenumber spectra in Drake Passage. *Journal of Physical Oceanography*, *46*, 601–620.
- Savage, A. C., Arbic, B. K., Alford, M. H., Ansong, J. K., Farrar, J. T., Menemenlis, D., et al. (2017). Spectral decomposition of internal gravity wave sea surface height in global models. *Journal of Geophysical Research: Oceans*, *122*, 7803–7821. <https://doi.org/10.1002/2017jc013009>
- Shakespeare, C. J., & Hogg, A. M. (2017). Spontaneous surface generation and interior amplification of internal waves in a regional-scale ocean model. *Journal of Physical Oceanography*, *47*(4), 811–826.
- Shriver, J. F., Arbic, B. K., Richman, J. G., Ray, R. D., Metzger, E. J., Wallcraft, A. J., & Timko, P. G. (2012). An evaluation of the barotropic and internal tides in a high-resolution global ocean circulation model. *Journal of Geophysical Research*, *117*, C10024. <https://doi.org/10.1029/2012jc008170>
- Simpson, J. H., Hyder, P., Rippeth, T. P., & Lucas, I. M. (2002). Forced oscillations near the critical latitude for diurnal-inertial resonance. *Journal of Physical Oceanography*, *32*(1), 177–187.
- Su, Z., Wang, J., Klein, P., Thompson, A. F., & Menemenlis, D. (2018). Ocean submesoscales as a key component of the global heat budget. *Nature communications*, *9*(1), 775.
- Torres, H. S., Klein, P., Menemenlis, D., Qiu, B., Su, Z., Wang, J. B., et al. (2018). Partitioning ocean motions into balanced motions and internal gravity waves: A modeling study in anticipation of future space missions. *Journal of Geophysical Research: Oceans*, *123*, 8084–8105. <https://doi.org/10.1029/2018jc014438>
- Wang, J., Fu, L. L., Qiu, B., Menemenlis, D., Farrar, J. T., Chao, Y., et al. (2018). An observing system simulation experiment for the calibration and validation of the surface water ocean topography sea surface height measurement using in situ platforms. *Journal of Atmospheric and Oceanic Technology*, *35*(2), 281–297.
- Wang, J., Fu, L. L., Torres, H. S., Chen, S. M., Qiu, B., & Menemenlis, D. (2019). On the spatial scales to be resolved by the Surface Water and Ocean Topography Ka-band radar interferometer. *Journal of Atmospheric and Oceanic Technology*, *36*(1), 87–99.
- Yuan, X. (2004). High-wind-speed evaluation in the Southern Ocean. *Journal of Geophysical Research*, *109*, D13101. <https://doi.org/10.1029/2003jd004179>
- Zaron, E. D. (2019). Baroclinic tidal sea level from exact-repeat mission altimetry. *Journal of Physical Oceanography*, *49*(1), 193–210.
- Zhang, Z., & Qiu, B. (2018). Evolution of submesoscale ageostrophic motions through the life cycle of oceanic mesoscale eddies. *Geophysical Research Letters*, *45*, 11,847–11,855. <https://doi.org/10.1029/2018gl080399>
- Zouari, N., & Babiano, A. (1990). Lagrangian numerical experiments based on Eulerian models. *Atmosphere Ocean*, *28*, 345–364.